Chapter 4

Accumulation, Storage and Manipulation of Large Numbers of Positrons in Traps I. – The Basics[a]

Clifford M. Surko

University of California, San Diego,
La Jolla CA 92093, USA
csurko@ucsd.edu

In this chapter, methods are described to create, store, manipulate and characterize positron plasmas. Emphasis is placed on the so-called buffer-gas positron trapping scheme for positron accumulation that uses positron-molecule collisions to accumulate particles efficiently. Manipulation and storage techniques are described that exploit use of the Penning–Malmberg trap, namely a uniform magnetic field with electrostatic confining potentials along the direction of the field. The techniques described here rely heavily on single-component-plasma research, and relevant connections are discussed. The use of rotating electric fields to compress plasmas radially (the so-called "rotating-wall" technique) is described; it has proven particularly useful in tailoring positron plasmas for a range of applications. The roles of plasma transport and available cooling mechanisms in determining the maximum achievable plasma density and the minimum achievable plasma temperature are discussed. Open questions for future research are briefly mentioned.

[a] This chapter, with corrections and minor updates as noted, is reprinted with permission from *Proceedings of the International School of Physics "Enrico Fermi*", "Physics with Many Positrons", Course CLXXIV, in Brusa, R. S., Dupasquier, A., Mills, A. P., Jr. (eds), (IOS Press, Amsterdam, 2010), pp. 511 – 543.

4.1. Overview

The School on Physics with Many Positrons,[a] for which this and a companion[1,2] chapter were written, highlighted the fact that progress in the ability to accumulate and cool positrons and antiprotons is enabling new scientific and technological opportunities with low-energy antimatter. In a major sense, much of this work has its origins at the forefront of plasma physics research – the development of new ways to create and manipulate antimatter plasmas. These chapters describe the development of new plasma tools for this effort. Thus, they also fit well in this volume of lectures from the 2012 Les Houches Winter School on Physics with Trapped Charged Particles. The objective of these chapters is to provide a description of methods to efficiently accumulate, store and manipulate positrons in the form of single-component plasmas for use in a variety of applications. Aspects of these techniques are also relevant to the confinement and manipulation of antiprotons.[b]

Chapter 5 describes recently developed methods of creating positron beams with small transverse spatial extent. The prospects for accumulating and storing larger quantities of antimatter are also discussed in Chapter 5, namely a novel multicell positron trap capable of storing $\geq 10^{12}$ positrons for days or longer, as well as other selected topics. These chapters are intended to be tutorial in nature rather than a first description of research results. They borrow heavily from previously published material, sometimes repeating passages verbatim. This chapter relies heavily on the material in references[3–5]. The reader is requested to consult these and other original articles for further details.

Single-component plasmas (SCP) are the method of choice to accumulate, cool and manipulate large numbers of antiparticles. These collections of antimatter can be stored in a high quality vacuum for very long times using the suitably arranged electric and magnetic fields of a Penning–Malmberg trap[6] – this device functions as a nearly ideal

[b] There are, however, significant differences. Due to the antiproton's annihilation characteristics and heavier mass, the positron cooling techniques described here must be replaced, cooling the antiprotons sympathetically with cold electrons. Further, the accumulations of antiprotons to date have typically been gases of charged particles rather than plasmas.

electromagnetic bottle. Not only can these positron plasmas be made more or less arbitrarily free of annihilation, but, in addition, techniques are available to further cool, compress, and tailor them for specific applications. These antimatter plasmas now play an important role in science and technology and this is expected to continue.

Low-energy antimatter science relies upon many developments in positron technology. They include methods to cool plasmas rapidly using specially chosen buffer gases[7] or cyclotron emission in a large magnetic field;[8] the application of rotating electric fields for radial plasma compression;[4,5,7,9–11] the development of non-destructive diagnostics using plasma waves[11–13]; and the creation of beams of small transverse spatial extent by careful extraction from trapped and cooled antimatter plasmas.[14–16]

There are numerous applications of these positron plasmas and trap-based beams. Trapped positron plasmas and similarly confined clouds of antiprotons are the method of choice to make low-energy antihydrogen atoms.[11,17–20] One goal of that work is to test fundamental symmetries of nature by precision comparisons of hydrogen and antihydrogen. Attempts are being made to create and study electron–positron plasmas that are of interest in plasma physics and astrophysics.[21–24] Bursts of positrons from a trap-based beam were used to create the first positronium molecules (Ps_2). This represents an important step toward the creation of a Bose–Einstein condensate (BEC) of Ps atoms.[25] Positrons have been used extensively to study materials,[26–28] such as low dielectric constant insulators that are key components in high-speed electronics and chip manufacture.[28] An important focus of recent work is the further development of pulsed, trap-based positron beams that offer improved methods to make a variety of materials measurements. Commercial prototypes of these beam systems are now available.[29,30] Positrons are also important in medicine and biology; positron emission tomography is the method of choice to study metabolic processes in humans and animals, both to treat disease and to develop new therapies.[31] In the longer term, research in this area may well lead to the development of *portable* antimatter traps, and this, in turn, would facilitate many other uses of antimatter.[3,32]

Much of the following discussion relies on the physics of single–component plasmas in Penning–Malmberg (PM) traps, namely a plasma in a cylindrical set of electrodes immersed in a uniform magnetic field with electrostatic confinement along the direction of the field. Relevant parameters to describe these plasmas and the notation used here and CCII are listed in Table 4.1.[c] The book by R. C. Davidson[33] and the review article by Dubin and O'Neil[34] contain excellent, detailed discussions of the theoretical plasma physics concepts relevant to non-neutral plasmas, including those in PM traps.

4.2. Positron Trapping

Background and overview. In our world of matter, positrons are typically produced using accelerators or radioisotopes. To be trapped, they must be slowed to electron-volt energies from their initial, broad spectrum of energies, ranging from several kiloelectron-volts to ~ 0.5 MeV. Typically a "moderator" material is used to slow them down. This is done by either transmission through or reflection from a metal, such as single-crystal copper or tungsten (energy spread ~ 0.5 eV; efficiency $\leq$ 0.1 %),[26,35] or reflection from a frozen, solid rare gas such as neon (energy spread ~ 1 eV; efficiency $\geq$1 %).[36,37] These materials are chosen specifically for the characteristic that positrons do not readily bind to them or become trapped in voids or at defects. In particular, some metals have a negative positron work function and can be grown in large single crystals; they are thus well suited for positron moderation.

The accumulation and confinement of positrons in electromagnetic traps has a long history. In the early 1960s, Gibson, Jordan and Lauer injected radioactive neon gas in a vacuum chamber surrounded by magnetic mirror coils.[38] The emitted positrons were confined by the mirror field. The escape time, relative to the Ne gas puff, was used to measure the single-particle confinement time. Schwinberg, Van Dyck and Dehmelt confined small numbers of positrons in a Penning trap for very long times (weeks to months).[39] Their goal was to make precision

[c] Expressions in this chapter are in S. I. units, unless otherwise noted. In these units, ε_0 is the permittivity of free space.

comparisons of the properties of electrons and positrons. Mills and collaborators used a Penning trap to confine and bunch positrons from a radioisotope source[40] and from a microtron accelerator[41] for use in spectroscopic studies of Ps atoms. Brown, Leventhal, Mills and Gidley confined positrons in a Penning trap to measure the annihilation Doppler broadening spectrum of molecular hydrogen in order to model astrophysical annihilation spectra.[42] In all of these experiments, small numbers of positrons were confined at low densities (i.e., typically in the positron–gas regime rather than the plasma regime). Here we focus on the accumulation of large numbers of positrons in the plasma regime.

Table 4.1. Parameters used to describe single-component plasmas in PM traps.[2] See text for details. The symbols m and e are the positronic mass and charge, respectively, with the sign of e positive.

Quantity	Symbol	Formula	Units
temperature	T	–	eV
number density	n	–	m^{-3}
plasma length	Lp	–	m
thermal velocity	v_T	$(T/m)^{1/2}$	m s^{-1}
cyclotron frequency	ω_c	eB/m	rad s^{-1}
cyclotron cooling rate	Γ_c[d]	$B^2/4$	Hz
plasma frequency	ω_p	$(ne^2/\varepsilon_0 m)^{1/2}$	rad s^{-1}
cyclotron radius	r_c	v_T/ω_c	m
Debye screening length	λ_D	v_T/ω_p	m
axial bounce frequency	f_b	$v_T/2L_p$	Hz
ExB rotation frequency	f_E	$\frac{ne}{4\pi\varepsilon_0 B}$	Hz
Brillouin density limit	n_B	$\varepsilon_0 B^2/2m$	m^{-3}

[d] Γ_c is used as the cooling rate, independent of the specific technique (e.g., for collisional cooling also). The formula displayed here is for cyclotron cooling with B in tesla.

While a number of devices and protocols have been used or proposed to trap antimatter, the device of choice is the PM trap because of its excellent confinement properties. Other variations of the Penning trap that have either been discussed or employed to trap antiparticles and antimatter plasmas include hyperboloidal,[39] orthogonalized cylindrical[43] and multi-ring electrode structures.[44] The PM trap is illustrated in Figure 4.1. It uses a uniform magnetic field to inhibit the diffusion of particles across the B field and an electrostatic potential well, imposed by the application of suitable voltages on a set of cylindrical electrodes, to confine the particles in the direction of the B field.[34,45,46] The extremely long confinement times that can be achieved in these traps[6,47] makes the accumulation of substantial amounts of antimatter feasible in the laboratory.

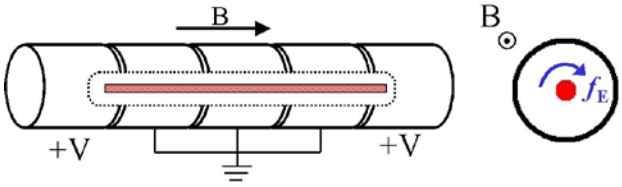

Fig. 4.1. Schematic diagram of a PM trap. The plasma is shown in the cutaway section. It is confined by a uniform axial magnetic field and by the electrostatic potential, V, at each end. As described below, the plasma rotates about its axis with an E x B frequency f_E, as illustrated in the end-on view (right).

An efficient accumulation scheme – the buffer-gas trap. Given this good trapping scheme, the challenge is to find an efficient method to fill the trap with positrons. A variety of trapping techniques have been developed to do this. If a pulsed positron source such as as a linear electron accelerator (LINAC) is used, the positrons can be captured by timed switching of the potential on one of the end confining electrodes. This end-gate switching technique has been employed extensively to condition positron beams from LINACs and other pulsed sources.[48] It has also been used to transfer positrons from one trap to another.[20,49,50] For high capture efficiency, the spatial extent of the incoming pulse must be smaller than twice the trap length, and the slew rate on the capture

gate must be sufficiently rapid. In many circumstances, these conditions are relatively easy to meet.

When positrons are captured from a steady-state source, such as a radioisotope, energy can be extracted from the positrons to trap them, or energy can be transferred from the positron motion in the direction parallel to the magnetic field to the perpendicular direction by a variety of techniques. The latter effect results in "virtual trapping" in that the particles can subsequently be de-trapped by the reverse process. A variety of techniques have been developed to trap positrons using these approaches, including collisions with neutral gas atoms and molecules[51, 52], scattering from trapped ions,[39,53] scattering from trapped electrons in a nested potential well,[54] and trapping in a magnetic mirror.[55] Other methods used to trap positrons include using dissipation in an external resistor,[56] field ionization of weakly bound positronium (Ps) atoms[53,57] and the exchange of parallel and perpendicular momentum exploiting stochastic orbits.[58] Each of these techniques has its advantages, but it turns out that they are relatively inefficient.

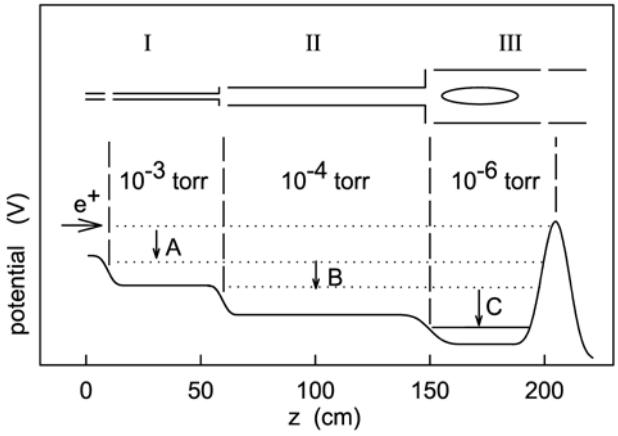

Fig. 4.2. Buffer-gas trapping scheme, showing the electrode geometry of a modified PM trap (above), the neutral gas pressure in each stage and the axial potential profile (below). There is an applied magnetic field, B ~ 0.15 T, in the z direction. Two-stage accumulators with B as small as 0.04 T have also been used successfully.[59]

The positron trapping method most widely used is the buffer-gas (BG) technique. It has the highest trapping efficiency and modest magnetic

field requirements. Figure 4.2 illustrates the operating principle of such a buffer-gas positron accumulator which, in this example, has three stages.[52,60] Figure 4.3 shows the actual physical arrangement. Positrons are injected into a specially modified PM trap

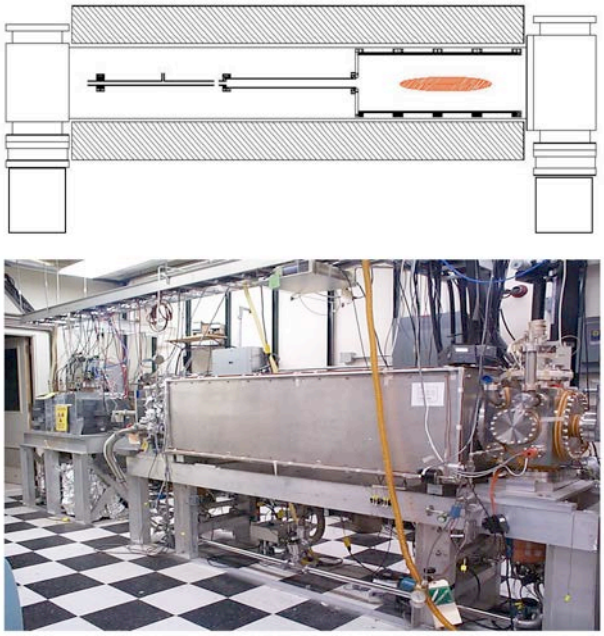

Fig. 4.3. A three-stage positron trapping apparatus with source and moderator at the University of California, San Diego (UCSD): (above) cutaway of a three-stage positron trap; (below) photograph of the positron source (a sealed ^{22}Na radioisotope source and solid neon moderator) in a lead enclosure at the left, and the three-stage trap in the large metal box on the right. For spatial scale, the floor tiles are ~ 0.3 x 0.3 m.

having a stepped potential profile, with each stage having a different pressure of buffer gas. Using a continuous gas feed and differential pumping, a high pressure (~10^{-3} mbar) is maintained in the small-diameter region at the left (stage I in Figure 4.2). Positrons are initially trapped in this region by inelastic collisions with buffer-gas molecules (marked "A" in Figure 4.2). The trapped positrons then make multiple

passes back and forth in the trap. They lose energy by subsequent inelastic collisions ("B" and "C") in the successively lower pressure stages II and III, causing them to accumulate in stage III. Here, they cool to approximately the gas (i.e., the electrode) temperature, which is ~ 300 K.

This type of accumulator can be operated using a variety of gases including molecular nitrogen, hydrogen, carbon dioxide and carbon monoxide.[29] There are two considerations regarding the choice of buffer gas. One is to find a target species that has a relatively large cross-section for energy loss via inelastic scattering. The second is to avoid Ps atom formation, which results in loss of positrons through annihilation, either in the Ps atom or when the Ps strikes an electrode or the vacuum chamber.

It would be appealing to use the vibrational excitation of molecules for this energy loss process, however this results in a loss per collision ≤ 0.5 eV. In practice, this is too small to efficiently trap the spread of positrons from the moderator (e.g., energy spreads ~ 1 eV). An important effect is due to the fact that typical source/moderators are operated at a reduced magnetic field (typically $B \leq 0.03$ T). The quantity $E_{\perp}/B$ is an adiabatic invariant for these particles, where $E_{\perp}$ is the energy in motion in the plane perpendicular to B. Thus, when particles with a spread of $E_{\perp}$ values enter the higher magnetic field of the BG trap, the spread in parallel energies, $E_{||}$, increases significantly. This generally reduces the trapping efficiency since the inlet potential cannot be as carefully tuned so that incoming positrons just pass over it. The entire spread of $E_{||}$ must now pass over the inlet potential barrier of the trap. Positrons with larger values of $E_{||}$ must lose correspondingly more energy before they become trapped, and it is more difficult to tune the potential steps to optimize the energy loss per collision for all of the particles.

The highest trapping efficiency is obtained using molecular nitrogen. The reason it is superior is that, as shown in Figure 4.4, this species has a relatively large electronic excitation cross-section at positron impact energies ~ 10 eV, near the threshold for electronic excitation of the $a^1\Pi$ of N_2 at 8.8 eV,[61] while it also has a relatively small cross-section for Ps formation (i.e., a potent positron loss process) in this range of energies.

To our knowledge, molecular nitrogen is somewhat unique in this important characteristic. In most other molecules, the Ps formation threshold is below that for the lowest allowed inelastic electronic transition.

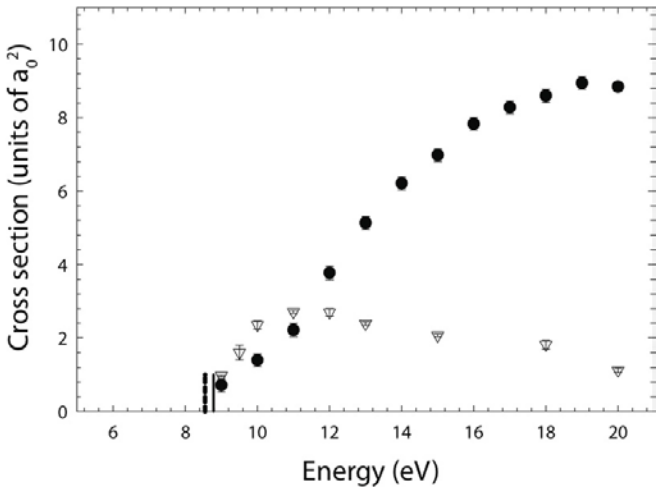

Fig. 4.4. Cross-sections in atomic units (a_0^2 = 2.8 x 10^{-21} m^2) for positron-impact excitation of the $a^1\Pi$ electronic state of N_2 (∇) and Ps formation ($\bullet$). The dashed and solid vertical bars indicate the thresholds for electronic excitation and Ps formation, respectively. From reference[61].

The pressure in stage I is set so that the positrons make, on average, ~ one electronic-excitation collision in one transit through the trap and hence are confined in the potential well. This happens before they reflect off the potential barrier at the end of the trap opposite the source, exit the trap, and return to the moderator, where they would be lost to annihilation. Once trapped, the positrons move back and forth in the direction of the magnetic field. Additional stages with stepped potentials and correspondingly lower neutral gas pressures (i.e., two more stages in the trap illustrated in Figure 4.2) are arranged to trap the positrons in a region of low gas pressure in which the annihilation time is commensurately long. The positron lifetime in stage III of the trap illustrated in Figure 4.2 is typically $\geq$ 40 s. Longer lifetimes (e.g., hours

or more) can be achieved by pumping out the buffer gas following positron accumulation.

While N_2 has a relatively large electronic excitation cross-section, its vibrational excitation cross-section is quite small. The addition of a low pressure (e.g., $\leq 10^{-7}$ mbar) of CF_4 or SF_6 in stage III is used to cool rapidly to room temperature.[9] The unusually large positron-impact vibrational cross section of carbon tetrafluoride,[62] which is discussed in more detail below, is responsible for rapid cooling to temperatures ≤ 0.16 eV, and SF_6 is believed to act similarly. For the typical pressure settings in the three-stage trap shown in Figure 4.3, operating with N_2 in stages I – III and CF_4 in stage III, the positrons are trapped in one transit back and forth through the trap. They lose additional energy by a second electronic excitation of N_2 and are thus confined in stages II and III in $\leq$ 100 μs. The positrons then make a similar collision in stage III and are confined to this stage in a few ms.[52] Finally, the positrons cool to room temperature by vibrational and rotational excitation of CF_4 in ≤ 0.1 s. A set of rate equations describing this cascade to lower positron energies is discussed in reference[52].

For accumulators with a solid neon moderator, the trapping efficiencies (i.e., defined as the fraction of positrons trapped and cooled relative to the number of incident slow positrons from the moderator) are typically in the range of 5–20%, and efficiencies of up to 30% have been observed under optimized conditions. Using a tungsten moderator, the efficiency can be as high as 50%. While not studied in detail, the trapping efficiency is likely limited by Ps atom formation and the small positron density in the first stage of the trap. This positron-density effect, which is discussed in more detail below, is due to $\tilde{E}xB$, asymmetry-induced radial transport, where $\tilde{E}$ is the (DC (direct current) in the laboratory frame) electrostatic field due to trap asymmetries. It is largest in the first trapping stage where the positron density is the smallest.

Using a 100 mCi ^{22}Na source and solid neon moderator, several hundred million positrons can be accumulated in a few minutes in the three-stage trap shown in Figure 4.3.[63] Once accumulated, the resulting positron plasmas can be transferred efficiently to another trap and stacked (e.g., for long-term storage).[20,49,50] Figure 4.5 shows the history

of positron trapping using apparatus such as those described here using similar strength sources.

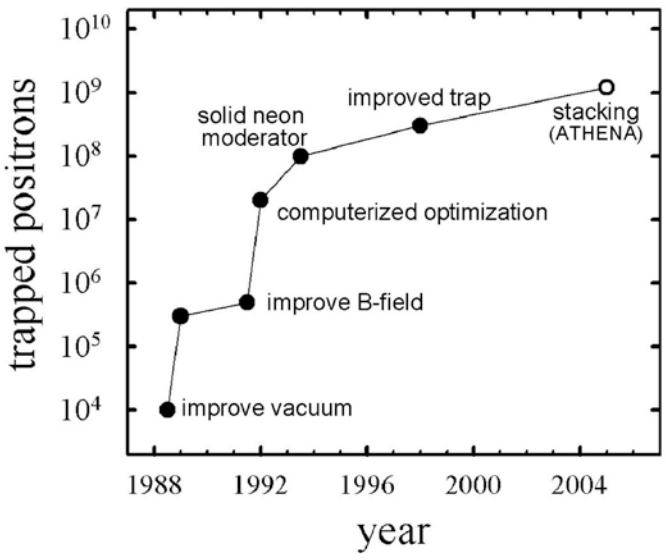

Fig. 4.5. Progress in creating positron gases and plasmas in PM traps using ^{22}Na positron sources with strengths ~ 50 – 100 mCi. For the data before 1993, tungsten moderators were used, while after that, solid neon moderators were used.

These buffer-gas traps are relatively efficient, arguably even efficient on an absolute scale. The difference between 5% and 30% efficiency is typically due to the fine tuning of the alignment of the incoming positron beam with respect to the electrode structure. In this regard, careful choice of the inner diameter of the first stage electrodes and operating pressure is likely of considerable importance. One area that, to the author's knowledge, has not been explored extensively is the extent to which elastic scattering on atoms or molecules (i.e., transfer of parallel energy to that perpendicular to the B-field), and the resulting process of virtual trapping could be used to advantage, particularly in the first stage of the buffer-gas trap. In this process, the particles will be trapped until another elastic scatter de-traps them, or an inelastic collision traps them absolutely.

Simpler, two-stage positron accumulators with correspondingly shorter positron lifetimes (e.g., ≤ 1 s) have now been developed.[59,64] Commercial two- and three-stage positron traps, such as that shown in Figure 4.6, are now sold commercially by R. G. Greaves at First Point Scientific, Inc., Agoura Hills, CA.

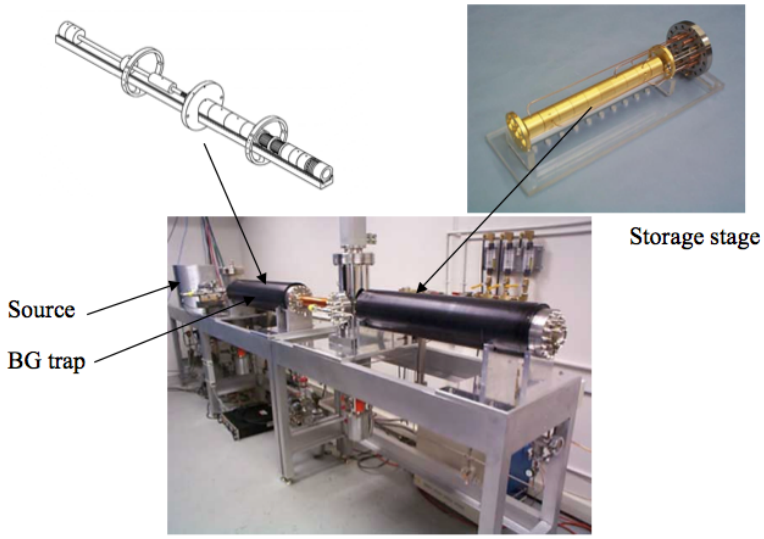

Fig. 4.6. A commercial two-stage buffer-gas trap and a separate storage stage (i.e., a three-stage system) with a ^{22}Na source and solid neon moderator. (below) Photograph of the system; with, left to right, the source/moderator (in the shiny cylinder), (in the black solenoids) the buffer-gas trap and the storage stage. Also shown are (top left) the buffer-gas trap electrodes, and (top right) the storage stage electrodes. Courtesy of R. G. Greaves, First Point Scientific, Inc., Agoura Hills, CA.

We end this discussion with a cautionary practical note about positron traps such as those described here. It is well known that positron annihilation rates on large hydrocarbon molecules can be extremely high. This arises from the fact that positrons tend to bind to these species (i.e., through a mechanism known as vibrational Feshbach resonances).[65] Oil molecules are particularly deleterious in this regard. Thus considerable care must be taken in achieving a good, oil-contaminant-free base vacuum in the accumulator (e.g., ≤ 5 x10^{-10} mbar) and/or trap. The

vacuum system should be bakable (e.g., to 420 K or higher), if long confinement times are desired.

4.3. Positron Cooling

Moderator materials (as described above) are used to decelerate high-energy positrons from a source to electron-volt energies. Once accumulated in a PM trap, these collections of charged particles can be heated by small electric perturbations. This is quite deleterious to positron confinement for a number of reasons. For example, heating to above the energy threshold for Ps formation leads to a first-order particle loss. Furthermore, increased positron energy can also lead to de-confinement. Thus arranging an effective method to cool these positron gases and plasmas is extremely important. This is absolutely obligatory in cases where the plasma can be heated substantially. Such heating can occur, for example, when rotating electric fields are used to compress plasmas radially, or when there is a manipulation of positron gases and plasmas between various trapping regions.

Collisional cooling using atomic or molecular gases. At electron-volt energies and below, positron cooling can be accomplished by collisions with suitable gases of atoms or molecules. This was described briefly above, but a bit more amplification is in order. The cooling gas is selected to have a large inelastic scattering cross-section in order to achieve significant energy loss. However *positron loss* due to Ps atom formation must be avoided if possible. So-called "direct" annihilation of a positron with a bound electron in an otherwise elastic collision typically has a much smaller cross-section. Thus, where possible, one tries to work below the threshold for Ps formation (i.e., which can be several electron-volts or more). In fact, to avoid loss due to Ps formation with positrons on the tail of the Maxwellian distribution, the positron temperature should be kept a factor of three or more below the Ps formation threshold (e.g., $T \leq 2$ eV). For relatively low positron temperatures, direct annihilation then becomes an important factor in determining the lifetime of trapped positrons (e.g., ~ 40 s for N_2 at a pressure ~ 10^{-6} mbar).

Only recently have state-resolved inelastic positron-impact cross-sections been measured;[65] and so a general, quantitative understanding of the collisional positron cooling processes involving atoms and molecules is not available. Typically at energies in the electron-volt range, electronic transitions can be used to reduce the positron energy effectively. At energies in the range from 50 meV to those of the electronic transitions, vibrational transitions in molecules can be used, while below ~ 0.05 eV, one must rely on rotational transitions in molecules and momentum-transfer collisions with atoms to cool the positrons.

In the case where a single inelastic scattering channel is relevant (e.g., a vibrational mode *j* with energy ε_j), the cooling rate Γ_c will be,

$$\Gamma_c \equiv \frac{1}{T} dT/dt \approx -\frac{\nu_j \varepsilon_j}{T}, \tag{4.1}$$

where ν_j is the excitation rate for this transition. As we discuss in more detail below, this collisional cooling rate is applicable if there are no heating electric fields. If there are heating fields, then any momentum-transfer (e.g., an elastic) collision can convert the coherent field-driven component of the kinetic energy into heat, and this must be taken into account to determine the net cooling/heating rate. Such a detailed account of scattering processes is beyond the scope of this review. Likely Monte Carlo computer calculations would be useful in studying this balance of heating and cooling,[66] assuming the necessary collisional cross-sectional data are available.

Cross-sections for vibrational excitation of molecules have now been measured for several species,[67,68] and at least a semi-quantitative understanding of the magnitudes of these cross-sections is available.[69] Moreover, positron-cooling rates due to vibrational excitation have been measured for several molecules.[7,29,70] Cooling rates for selected molecules are given in Table 4.2. It turns out that SF_6 and CF_4 are particularly effective. In these species, there is a large amount of charge transfer to the F atoms. This results in a very large vibrational excitation

Table 4.2. Positron cooling rates in a PM trap using molecular gases at 2.6 x 10^{-8} mbar: time τ_a, for direct annihilation; measured cooling time, τ_c; and the energies of the vibrational quanta, ε_j. Data from references[7,9].

Gas	$\tau_a(10^3$ s)	τ_c(s)	ε_j(eV)
SF_6	2.2	0.36	0.076, 0.19
CF_4	3.5	1.2	0.16
CO_2	3.5	1.3	0.29, 0.083
CO	2.4	2.1	0.27
N_2	6.3	115	0.29

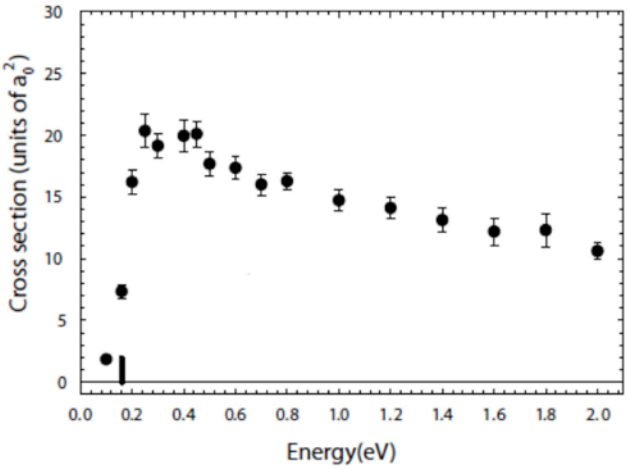

Fig. 4.7. Positron-impact cross-section for excitation of the ν_3 vibrational mode of CF_4 as a function of incident positron energy in atomic units (a_0^2 = 2.8 x 10^{-21} m^2). The relatively large and approximately constant cross-section above the threshold energy, ε_j = 0.157 eV, provides a very efficient and useful cooling mechanism. Reprinted from reference[62].

cross-section for the asymmetric stretch (i.e., ν_3) vibration in the molecule. Shown in Figure 4.7 is the cross-section for the ν_3 mode of CF_4.[62]

The current versions of buffer-gas positron traps typically use a mixture of N_2 and CF_4 or SF_6 in the final trapping stage for rapid cooling. There is very little information available on positron energy loss due to rotational excitation of molecules, save for an early study by Coleman *et al*. using a positron lifetime technique,[71] thus this would likely be a fruitful area for future work. As discussed below, CF_4 has also been used effectively for the cooling required for the radial compression of positron plasmas (i.e., to counteract the heating caused by the work done on the plasma by the applied torque).

Cyclotron cooling. A convenient method to cool electron-mass charged particles (positrons) in an ultra-high vacuum (UHV), is to arrange for them to emit cyclotron radiation in a strong magnetic field.[47] In this case, the positron temperature is typically a balance of heating (e.g., RF (radio frequency) electric fields are particularly effective in this regard) and the cyclotron cooling. In fact, cyclotron cooling at achievable magnetic fields is typically considerably less effective than cooling using gaseous collisions; so in this case, heat sources can produce quite significant effects. In the absence of a heating source, the particles will come to equilibrium at the temperature of the surrounding electrode structure. However, in the case in which parts of the vacuum system are at higher temperatures (e.g., when the electrodes are cooled cryogenically), this can result in heating the plasma above the temperature of the electrode structure.[e] The cyclotron-cooling rate for electron-mass charged particles is,[47,72]

$$\Gamma_c \approx B^2/4, \tag{4.2}$$

where B is in tesla and Γ_c is in s^{-1}. For example, the radiative cooling time, $1/\Gamma_c$ of positrons in a 5 tesla field is 0.16 s. Assuming an emissivity, $\varepsilon = 1$, for the electrodes at the cyclotron frequency, the surrounding electrode structure is at temperature T_w, and there is no

[e] J. Fajans, Private communication, 2009.

external heating, the time dependence of the positron temperature, *T(t)*, of a positron plasma at initial temperature T_1 will be:

$$T(t) = T_0 + (T_1 - T_w)\exp(-\Gamma_c t). \tag{4.3}$$

Shown in Figure 4.8 is a typical cooling curve for the thermal relaxation of an electron plasma confined in an apparatus at 300 K.

Two comments are in order regarding cyclotron cooling in an electrode structure. If one can arrange a resonant cavity at the cyclotron frequency, then the cooling rate is increased by the Q factor of the cavity.[73] The second comment is that the electrode structure must have a minimum size in order for cyclotron cooling to be effective. In particular, the structure must be at least large enough to accommodate the lowest-order resonant mode. For a long circular electrode structure, this means the inner diameter of the structure must be $D \geq \lambda_c$, where λ_c is the electromagnetic wavelength at the cyclotron frequency. For smaller values of D, the electrodes will act as a waveguide beyond cutoff, and radiation by the particles will be suppressed.

Sympathetic cooling using ions. The techniques described above are limited to producing a temperature equal to the temperature of the environment, (e.g., 4 K for cyclotron cooling in a trap cooled to liquid helium temperature). However, laser cooling of ions in traps permits cooling to temperatures much lower than their surroundings. This technique has been used[53] to reach positron plasma temperatures significantly below the ambient by cooling the positrons sympathetically using laser-cooled ions that were simultaneously confined in the same trap with the positron plasma. Using this technique, a high-density positron plasma ($n = 4\times10^{15}$ m^{-3}) was cooled to < 5 K in a room-temperature trap. This technique has the potential to produce positron plasmas with parallel energies less than 100 mK.[f]

[f] At very large B fields and low temperatures, the perpendicular energy of the particles will eventually be limited by the energy of the lowest Landau level.

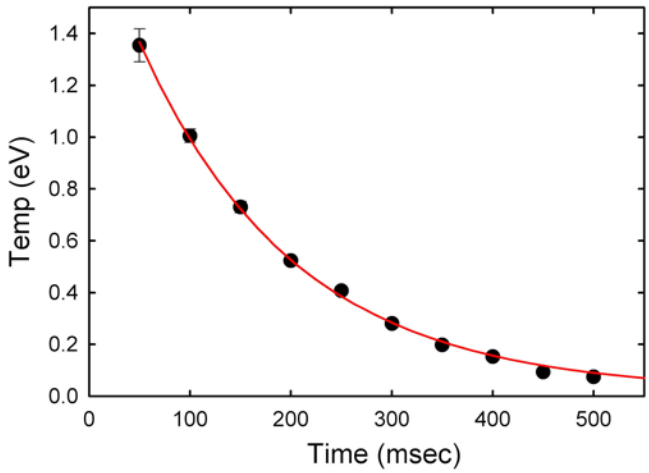

Fig. 4.8. Cyclotron cooling of an electron plasma in a magnetic field, B = 4.8 T, following heating with RF noise. Equation (2) yields Γ_c = 6.5 s^{-1}, compared with a predicted value of 5.9 s^{-1}. Courtesy of T. R. Weber, UCSD, unpublished.

4.4. Confinement and Characterization of Positron Plasmas in Penning–Malmberg Traps

Basic concepts. A typical PM trap for positrons is shown in Figure 4.9. It consists of a set of cylindrical electrodes in a uniform magnetic field. The plasma is confined in the direction of the magnetic field by electrostatic potentials applied to electrodes at each end. A segmented electrode over a portion of the plasma is used to apply a rotating electric field to compress the plasma radially (this is discussed in more detail in Section 4.5, below). Also shown is a phosphor screen and a CCD (charge-coupled device based) camera for imaging the radial distribution of the plasma[7] and the RF circuitry to excite waves in the plasma (e.g., for temperature and density measurements).[74,75]

In a single-component plasma at temperature T in the PM trap, the particles make only small excursions in the plane perpendicular to B. They are characterized by the (average) cyclotron radius, $r_c = v_T/\omega_c$, where the cyclotron frequency ω_c is the angular frequency of gyration of

the particle in the plane perpendicular to B, and $v_T = (T/m)^{1/2}$ is the average thermal velocity of the particle.

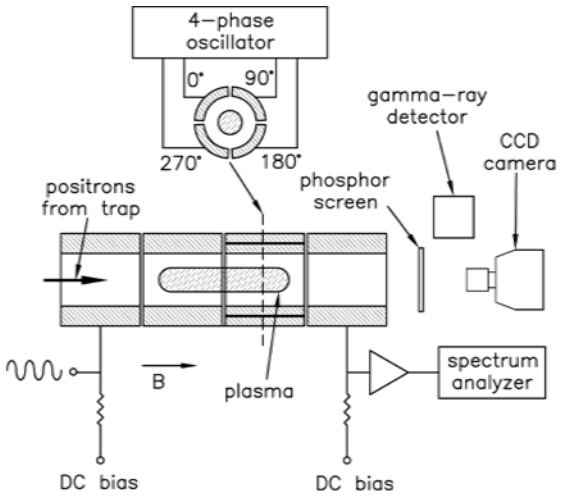

Fig. 4.9**.** Schematic diagram of a PM trap and associated apparatus for confining and manipulating positron plasmas. Shown is a segmented electrode for applying a rotating electric field for radial plasma compression, a phosphor screen and CCD camera for measuring radial density profiles and the electronics to excite plasma modes for diagnostic purposes.

They are subject to a confinement principle that arises from the fact that a charged particle in a B field has an angular momentum associated with it, beyond the ordinary mechanical momentum. As a consequence, at low temperatures where the thermal velocities of the particles are negligible, the canonical angular momentum P_θ[47] is approximately

$$P_\theta \approx -\frac{m\omega_c}{2}\sum_i r_i^2, \tag{4.4}$$

where the r_i are the radial positions of the particles, and it is assumed that the particles are positively charged which fixes the sign of P.

In a PM trap with cylindrically symmetric electrodes, the angular momentum, P_θ, is constant. Thus the second radial moment of the particle

distribution is also constant, and so the plasma cannot expand. In practice, these plasmas do expand slowly due to imperfections in the trap. In this case, the torque on the plasma is related to the outward transport rate, $\Gamma_0 = (1/n)(dn/dt)$, by

$$\tau = \frac{dP_\theta}{dt} = P_\theta \Gamma_0. \tag{4.5}$$

A single-component plasma in a PM trap is effectively a long cylindrical rod of charge. This collection of trapped particles will exhibit plasma behavior when the Debye length, $\lambda_D = v_{th}/\omega_p$, is such that $\lambda_D >> r_p, L_p$, where ω_p is the plasma frequency, r_p is the plasma radius and L the plasma length. In this case, potential perturbations in the plasma will be screened by motion of the particles in the direction parallel to B. Consequently, any remaining electric field in the plasma will be in the radial direction (i.e., neglecting end effects).

This radial electric field in and around the plasma results in a plasma potential that increases as one approaches the plasma center. From Gauss' law, for a long cylindrical plasma of N positrons with radius r_p in an electrode of radius r_w, the magnitude of this space-charge potential (i.e., the "plasma potential") at the plasma center is

$$\Phi = \frac{AN}{L}\left[1 + 2\ln(r_w/r_p)\right], \tag{4.6}$$

where $A = e/4\pi\varepsilon_0 = 1.4 \times 10^{-9}$ Volt–m. This value of Φ sets the minimum potential, V_c, required to confine the plasma, namely $V_c > \Phi$.

A key physical effect in PM traps and in other magnetized plasmas arises from the fact that the magnetic and electric space-charge fields are perpendicular to each other. This is illustrated in Figure 4.10 for a "slab" model that describes particle motion in two dimensions (i.e., ignoring the cylindrical symmetry of the PM trap). Charged particles in such fields undergo so-called "E x B drifts" at a velocity $v_E = E/B$, in the direction perpendicular to both E and B.[76,77] In terms of the cyclotron radius r_c and the characteristic distance $r_E = v_E/\omega_c$, the trajectories are "cycloids". Particles starting at the origin at time t = 0 orbit about a center *moving at*

velocity v_E, located at (x, y) position ($r_E + v_E t$, r_E), with an associated radius,

$$\rho = \sqrt{r_c^2 + r_E^2}\,. \tag{4.7}$$

In particular, the secular motion is in the x direction (i.e., perpendicular to both E and B), and the oscillation amplitude 2ρ is dominated by the larger of r_E and r_c. This latter effect has very important consequences for particle transport, namely the transport step size (~ ρ) can be dominated by r_E. Thus the transport can become very large when E is large (i.e, $v_E > v_T$), giving rise to large and rapid excursions of the particles outward.

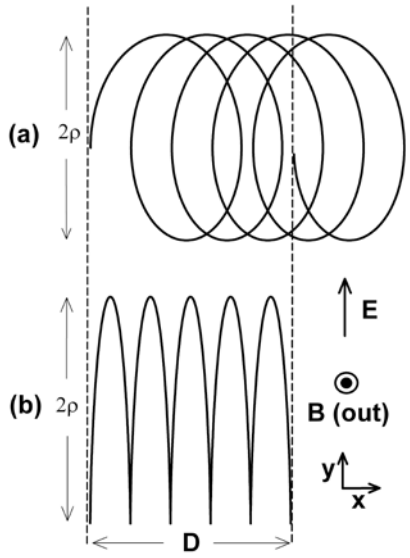

Fig. 4.10. E x B drift orbits for 5-cyclotron periods in a two-dimensional "slab" model (not to scale): (a) the usual drift-orbit case where the electric field is small, $r_E/r_c = 0.1$; and (b) a much larger electric field, $r_E/r_c = 10$. The corresponding radial excursions ρ and lateral distances (D) are approximately (a) r_c (πr_c), and (b) $10r_c$ ($100\pi r_c$). The particles make much larger excursions in the strong E field. (In the PM trap, y corresponds to the radial direction and x to the azimuthal direction.)

Due to the radial E field in the trapped plasma and the resulting E x B motion, the particles drift around the axis of symmetry at a frequency

$$f_E = \frac{ne}{4\pi\varepsilon_0 B}, \tag{4.8}$$

where n is the number density of the plasma. Note here the intimate connection between the rotation frequency, f_E, and the plasma density, n.

Transport due to neutral collisions. The angular momentum constraint of Eq. (4.4) implies that a single-component plasma confined by a magnetic field can expand only if there is a torque on it. In a perfect, azimuthally symmetric trap there would be no expansion. However in practice, this is not the case. Typically radial transport *is* observed. This can be due to trap imperfections, or, in the case where there is appreciable neutral background gas, this transport can be due to the drag on the plasma due to neutral collisions.[6,79]

The transport due to neutral gas collisions is reasonably well understood. In this case, the outward flux of particles (i.e., number of particles/area–time) J is,[6]

$$J = \frac{\partial}{\partial r}\left(\nu_p r_c^2 n\right) + \nu_p r_c^2\left(\frac{eE}{T}\right)n, \tag{4.9}$$

where ν_p is the positron-neutral, momentum-transfer collision frequency (frequently dominated by elastic scattering), and E is the space-charge electric field. The two terms in Eq. (4.9) are respectively the flux due to collisional diffusion, and the flux induced by the electric field that involves the electrical mobility of the plasma. In the plasma regime, $(eEr_p)/T >> 1$, and so the second term dominates the otherwise diffusive transport by a factor $\sim e\Delta\Phi/kT$, where $\Delta\Phi$ is the change in plasma potential across the plasma.[6] Assuming this is the case and inserting E for a rigid rotor, one finds for the outward transport rate, $\Gamma_0 \equiv (1/n)(dn/dt)$,

$$\Gamma_0 = \nu_p\left(\frac{r_C}{\lambda_D}\right)^2. \tag{4.10}$$

In the single-component positron (or electron) plasmas considered here, typically $r_c << \lambda_D$, and so the transport due to neutral-gas collisions is typically small.

Transport due to electric and magnetic asymmetries. In the case that gas collisions do not dominate the transport (e.g., a plasma in a UHV environment cooled by cyclotron radiation), a detailed, microscopic understanding of the transport has remained elusive in spite of 30 years research on the subject. It is believed to be due to azimuthal asymmetries. Recent studies point to the importance of so-called trapped particles and the influence of asymmetries upon them.[80] This somewhat subtle effect arises from the fact that particles trapped in electrostatic or magnetic wells (e.g., due to trap imperfections) do not experience the averaging effects that the bulk of the particles do, and so they can make larger radial excursions. When subsequently scattered out of this imperfection (i.e., trapping well), they can then cause greatly enhanced radial particle transport. From the perspective of antimatter-trap engineering, one typically relies upon empirical formulae based upon the now-extensive experimental studies. Data for the outward radial transport of particles (presumably due to asymmetries) from a plasma in a PM trap are shown in Figure 4.11.[81]

As shown in the Figure 4.11, there are two regimes of plasma transport. At sufficiently high plasma densities, Γ_0 is independent of n, whereas at lower densities $\Gamma_0 \sim (nL)^2$. The transition between these two types of behavior appears to occur when the axial bounce frequency, $f_b = v_{th}/2L_p$ is approximately three times the Coulomb collision frequency.[81] However, there is no theory at present for this effect, and it is unclear whether this result will hold in other experiments. The values of Γ_0 shown in Figure 4.11 are among the smallest values reported for the given parameters. In other experiments, Γ_0 can be as much as an order of magnitude greater, presumably due to larger trap asymmetries.[81] In practice, the best one can do to estimate the outward transport (and/or confinement time) is to use the reported values as order of magnitude estimates of the outward transport.

In considering the effects on transport due to electric asymmetries that are static in the laboratory frame, they are expected to be largest in plasmas with a small rotation frequency (i.e., in this case the transport is

due to asymmetry-induced E x B flows). However at higher rotation frequencies, the rotation can also bring the asymmetry-induced fields (that are DC in the laboratory frame) into resonance with a plasma mode. This can act as a potent drag on the plasma and result in a high level of transport.

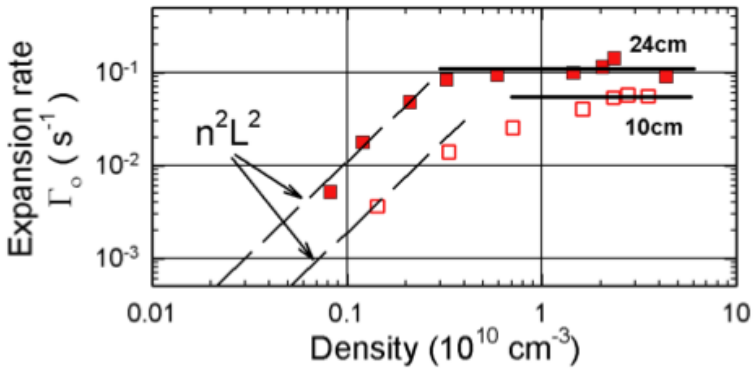

Fig. 4.11. The expansion rate, Γ_0, as a function plasma density for an electron plasma in a UHV PM trap in a 5-tesla field. The data show two regimes, including one in which Γ_0 is strongly density dependent. The transition occurs when the Coulomb collision frequency is ~ three times the axial bounce frequency. (In this figure, $L \equiv L_p$.) From reference[81]; see this reference for details.

The E x B transport at low rotation frequencies has important consequences for the operation of buffer-gas traps. In the first stages of a buffer-gas trap, or in traps confining small numbers of positrons, the rotation frequency will be small because the positron density is low. Thus, for example, a small static electrostatic asymmetry (e.g., arising from patch-voltages on the electrodes) can induce the rapid DC E x B transport of the particles to the wall. In the case of the buffer-gas trap, this means that one wants to get the particles out of these early trapping stages as quickly as possible and into the final stage where the plasma density (and hence the plasma rotation frequency) is higher. The small plasma rotation frequency in the first stage of buffer-gas traps can potentially play a significant role in limiting the trapping efficiency of these devices.

Plasma heating. Single-component plasmas in PM traps can be heated by various mechanisms, including ambient RF noise on the confining electrodes. One unavoidable heating source is the outward plasma expansion itself. Essentially, the radial, outward-directed electric field due to the plasma space charge preferentially gives the particles extra energy as they move outward radially. The heating rate, Γ_h, due to this effect can be written,[81–83]

$$\Gamma_h = \frac{1}{T}\frac{dT}{dt} = \left(\frac{e\phi_0}{2\eta T}\right)\Gamma_0, \tag{4.11}$$

where $1/\eta$ is the fraction of the space-charge potential that is dropped across the plasma, assuming $\phi = \phi_0$ at $r = r_w$. For a rigid-rotor plasma with a constant radial density profile, $\eta = \left[1 + 2\ln\left(a_w / r_p\right)\right]$, and ϕ_0 represents the potential drop across the plasma itself. Note that the plasma potential can be quite large (tens of volts are not atypical), so that in modestly cold plasmas, it can be the case that $\Gamma_h >> \Gamma_0$.

This heating must be mitigated by some type of cooling (e.g., cyclotron cooling or cooling due to collisions with gas molecules). In order for there to be a stable steady state, the heating rate must be smaller than the maximum cooling rate, i.e., $\Gamma_h/\Gamma_c < 1$, otherwise the temperature will increase in an uncontrolled manner.

If neutral collisions dominate both the transport and the cooling, we can combine Eqs (4.10) and (4.11) to find for the heating rate,

$$\Gamma_h = \frac{\nu_p}{4}\left(\frac{\omega p}{\omega c}\right)^2\left(\frac{r p}{\lambda D}\right)^2. \tag{4.12}$$

Neutral collisions with molecules can provide cooling via the excitation of vibrations (e.g., as is the case for CF_4). Considering the excitation of a single level, the cooling rate is given by Eq. (4.1). A measure of the effectiveness of this cooling can be obtained by forming the ratio, β, of the heating rate given by Eq. (4.12) to the cooling rate in Eq. (4.1). Thus,

$$\beta = \frac{\Gamma_h}{\Gamma_c} = \frac{\nu_p T}{4\nu_j \varepsilon_j}\left(\frac{\omega p}{\omega c}\right)^2\left(\frac{r p}{\lambda D}\right)^2. \qquad (4.13)$$

As discussed above, the plasma temperature will be stable only for $\beta \leq 1$, and will "run away" for larger values of η. Since $\beta \propto (n/B)^2$. *This places an important constraint on the maximum achievable plasma density n.*

It is useful to express the density in terms of the Brillouin limit density n_B (i.e., the density at which $\omega_p^2 = \omega_c^2/2$; see Eq. (4.19) and related discussion below for details), in which case,

$$\left(\frac{n}{n_B}\right)^2 = \frac{8\nu_j \varepsilon_j}{\nu_p T}\left(\frac{r c}{r p}\right)^2. \qquad (4.14)$$

Thus, to achieve high plasma densities, one would like a cooling gas with small ν_p and large ν_j. Carbon tetrafluoride fits this bill. As discussed above, it has an unusually large value of ν_j (cf., Figure 4.7[62]). It turns out that it also has a small value of ν_p,[84] making it a good choice for this purpose.

There are, however, two caveats regarding Eqs (4.12) – (4.14). Equation (4.14) is valid so long as the maximum density n is not very close to n_B. Close to the Brillouin limit, the cycloidal E x B orbits of the particles are very large and nearly unconfined, and a more careful calculation (not done here) is required. A practical criterion might be to set the amplitude of the cycloidal motion $\delta r = E/\omega_c B$ to be $\leq 0.1\ r_p$, which corresponds to $E/(\omega_c B r_p) \leq 0.1$ and $n/n_B \leq 0.1$. Further, we use particularly simple expressions for the collisional transport. Techniques such as Monte Carlo calculations would be very valuable in obtaining better estimates for the plasma expansion, heating and cooling.[66]

Diagnostic techniques. A variety of destructive and non-destructive techniques have been developed to measure the properties of non-neutral plasmas in traps, parameters such as plasma temperature, density, shape and the total number of particles. Destructive diagnostics involve releasing the particles from the trap and detecting them in various ways. Absolute measurements of the total number of particles can be made by

dumping the particles onto a collector plate and measuring the total charge.[6] In the case of positrons, the annihilation gamma rays can be detected when the particles are dumped, and the total particle number can thus be extracted using a calibrated detector. Radial profiles can be measured using a phosphor screen biased at a high voltage (~ 5 – 10 kV). The resulting fluorescent light is measured using a CCD camera.[85] Plasma density can be inferred from the radial profiles and the total number of particles can be calculated using a Poisson–Boltzmann equilibrium code.[86] Plasma temperature can be measured by releasing particles slowly from the trap and measuring the tail of the particle energy distribution.[87]

Destructive diagnostics have been employed extensively in the development of new techniques to manipulate and trap antiparticles. However, for experiments where the particles are collected for long periods of time, such as antihydrogen production or the creation of giant pulses, destructive diagnostics are disadvantageous. Several non-destructive techniques have been developed, based on the properties of the plasma modes. For long cylindrical plasmas, the frequency of the diocotron mode yields the charge per unit length of the plasma, and hence provides information about the total number of particles.[88,89]

For spheroidal plasmas in harmonic potential wells, the frequencies of the axial Trivilpiece–Gould modes[90] yield the aspect ratio of the plasma and can be used to measure plasma temperature in cases where the aspect ratio is constant.[11–13,74,91] Such a mode spectrum is shown in Figure 4.12. The total number of particles can be determined by the Q factor of the response,[13] or by independently calibrating the amplitude response.[12,74] Passive monitoring of thermally excited modes can also be used to determine the plasma temperature.[92] Driven-wave techniques have also been used to monitor positron plasmas used for antihydrogen production.[11,13] They were also applied to characterize electron plasmas that are used to trap and cool antiprotons.[93]

An important technique for manipulating non-neutral plasmas is to compress the plasma radially using a rotating electric field to apply a torque on the plasma. This is the so-called “rotating-wall” (RW) technique. It has provided important new capabilities for single-component plasma research, such as counteracting outward plasma

transport and permitting essentially infinite confinement times. It was first used to compress ion[94–97] and electron[82,98] plasmas. It has also been used to compress positron plasmas,[7,9] including those for antihydrogen production[11, 17, 99] and for the brightness-enhancement of positron beams.[14,15] This RW technique was also an important facet of the first successful creation of the positronium molecule, Ps_2.[25] It is expected to play a key role in work planned to produce giant pulses of positrons to create BEC of Ps atoms and the stimulated emission of annihilation radiation.[25]

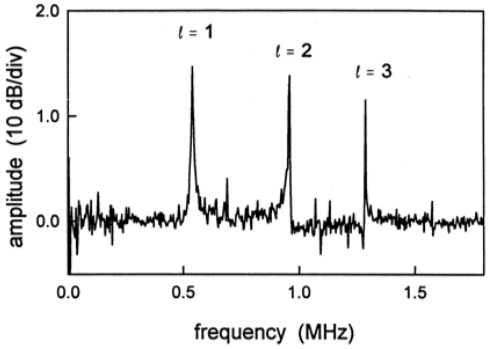

Fig. 4.12. Longitudinal compressional (Trivelpiece–Gould) modes of a positron plasma in a PM trap. From refence[74]; see this reference for details.

4.5. Radial Compression Using Rotating Electric Fields – the "Rotating-Wall" (RW) Technique

The process of RW compression involves coupling a rotating electric field to the plasma to inject angular momentum. As described by Eq. (4.4), this then reduces the second moment of the radial particle distribution.[47] The arrangement for RW compression is shown schematically in Figure 4.9. Phased sine waves applied to a sectored electrode are used to generate a rotating electric field with a low-order azimuthal mode number (e.g., $m_\theta = 1$).[7,9,10,81] These fields produce a torque on the plasma, thereby compressing the plasma radially in a non-destructive manner.

Efficient cooling is required to counteract the heating caused by the torque-produced work done on the plasma. As described above, this cooling can be provided by cyclotron cooling (in the case of a strong confining magnetic field),[10,11,13,81] a buffer-gas (in the case of a weak magnetic field),[7,9,100] or by sympathetic cooling using laser–cooled ions.[95]

Early RW experiments relied on coupling to (Trivelpiece–Gould) plasma modes, which significantly limited the utility and flexibility of the technique. Two RW operating regimes were later discovered in which tuning to plasma modes is unnecessary. The first was in a plasma with buffer-gas cooling when the plasma radius is comparable to the Debye length, λ_D.[9] The second was in plasmas in a high-magnetic-field trap when the drive amplitude is sufficiently large (the "strong-drive" regime).[81] Most RW compression experiments now operate (or try to operate) in this second, strong-drive regime.

Shown in Figure 4.13 is an apparatus for studying PM plasmas cyclotron cooled in a high magnetic field. Shown in Figure 4.14 is an example of compression of an electron plasma in this device in the strong-drive regime. The protocol for these experiments is such that *the RW is applied at fixed values of both V_{RW} and f_{RW}*. Above a certain drive amplitude, the plasma evolves to a high-density steady state in which $f_E \approx f_{RW}$ (cf. Figure 4.14). As illustrated in Figure 4.15, the radial density profiles of these plasmas are "flat-top" in shape (i.e., a constant-density rigid-rotor in a state close to thermal equilibrium). Experiments at various values of f_{RW} are shown in Figure 4.16, illustrating the ability to access a broad range of high-density states in this strong-drive regime.

The ability to access the strong-drive regime depends upon overcoming the drag due to static asymmetries in the laboratory frame. These asymmetries drive waves (i.e., Trivelpiece–Gould modes) traveling backwards on the rotating plasma and thus act as a drag on it. This is illustrated in Figures 4.16 and 4.17 where a "step" appears in the data near the density $n = 0.4 \times 10^{10}$ cm^{-3}. The mode frequency is zero in the lab frame and referred to as a "zero-frequency mode" (ZFM).[81] The

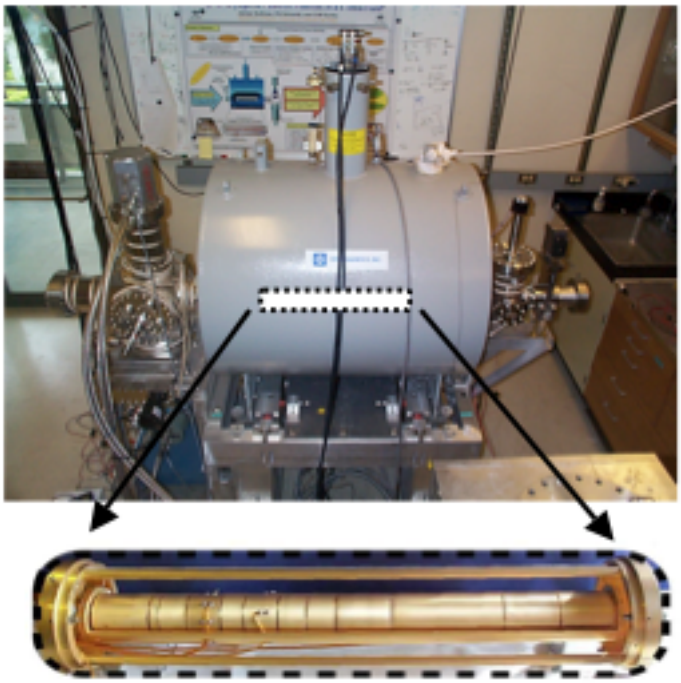

Fig. 4.13. A high-magnetic-field (5-tesla) UHV storage trap.[101] Also shown is a cutaway view of the electrode structure that contains two RW electrodes (left of center). The apparatus is also outfitted with a closed cycle pulsed-tube refrigerator for cooling the electrodes.

drag torques on the plasma have been modeled to include this ZFM effect,[5] namely the total torque on the plasma will be

$$\tau = \eta \frac{f_{RW} - f_E}{f_E} V_{RW}^2 - \frac{\beta f_E}{D^2 + f_E^{\,2}} - \frac{\gamma \delta f_0}{\left(f_E - f_0\right)^2 + \left(\delta f_0\right)^2} \quad , \quad (4.15)$$

where η, β, γ and D are constants. The terms in Eq. (4.15) represent the RW drive torque, τ_{RW} (first term) and the drag torques, τ_{drag}. The latter is the sum of the second and third terms, namely the background drag

torque (second term, coefficient β) on the plasma due to trap imperfections, and the drag due to the ZFM (third term, coefficient γ).

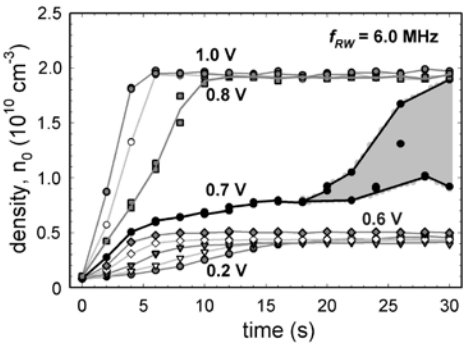

Fig. 4.14. Central electron density is shown as a function of time for various amplitudes of applied RW voltage at 6 MHz. Note the bifurcation from a low–density to a high density state as V_{RW} is increased above 0.7 V. Reprinted from reference[81].

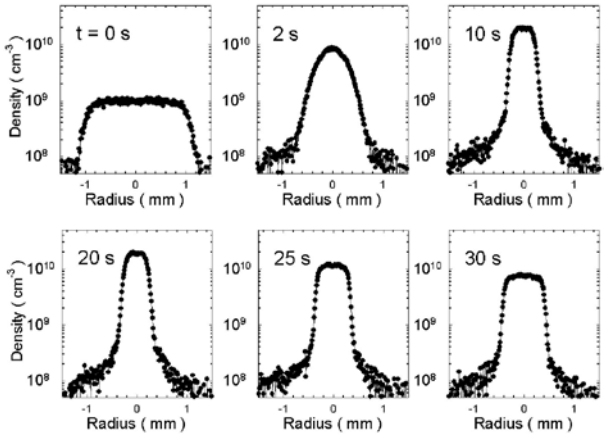

Fig. 4.15. Radial profiles for RW compression of an electron plasma in a 5-tesla magnetic field, using f_{RW} = 6 MHz, starting at t = 0 s. Steady-state compression is observed from t = 10 to 20 s, then the plasma expands with the RW off. Flat–top equilibrium profiles are observed, except at t = 2 s, where the plasma is hotter (i.e., T ~ 3 eV at that time). Reprinted from reference[81]; see this reference for details.

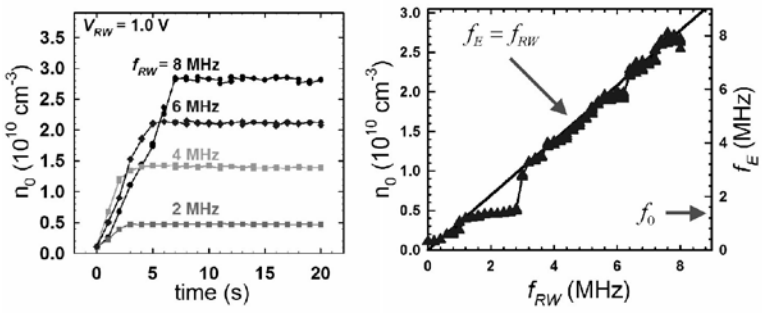

Fig. 4.16. (left) Central plasma density following application of the RW at various frequencies at V_{RW} = 1.0 V; and (right) steady-state density as a function of applied RW frequency, following the transition to the high-density state. The step near $n = 0.4 \times 10^{10}$ cm^{-3} is due to a so-called ZFM mode, which was key to understanding the high-density steady states. B = 5 T. Data from reference[81].

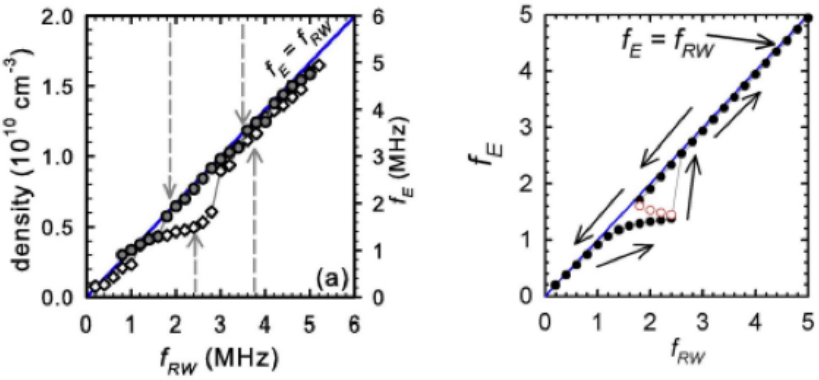

Fig. 4.17. (left) Density as a function of f_{RW}, when f_{RW} is fixed but the initial plasma density is smaller (upward arrow, ◊) or larger (downward arrow, ●) than that of the final, torque balanced steady states (i.e., the stable fixed points); (right) solutions of Eq. (4.13) for $\tau = 0$, for the (●) stable and (○) unstable fixed points when approached varying f_{RW} in the directions shown by the arrows. The model exhibits the same qualitative behavior as the data. Analysis from reference[5]; see this reference for details.

The form of the second term in Eq. (4.15) was chosen empirically to model the observed outward transport data such as that shown in Figure 4.11. An example of the drag torque derived from that data is shown in

Figure 4.18. The third term in Eq. (4.15) is the ZFM drag term, which is modeled by a Lorentzian of width δf_0, *centered* at frequency f_0. Equilibrium is reached when $\tau = 0$, and this condition sets the plasma rotation frequency, f_E.

This model for the total torque on the plasma yields predictions that agree well with experimental observations.[5] It turns out that, for suitably strong drives to overcome the ZFM drag, the plasma spins up until $f_{RW} \approx f_E$ (which, in the language of nonlinear dynamics, is an "attracting fixed point" of Eq. (4.15)). At lower values of τ_{RW}, the plasma becomes "stuck" at a rotation frequency close to that of the ZFM (i.e., the "low-density fixed point" at f_0). The stable state to which the plasma relaxes depends upon which side of the ZFM the plasma starts: the fixed point is stable when $d\tau_{RW}/df_{RW} > d\tau_{drag}/df_{RW}$ and unstable when $d\tau_{RW}/df_{RW} < d\tau_{drag}/df_{RW}$. As a consequence, the plasma is predicted to exhibit hysteresis as a function of the RW drive amplitude.

As shown in Figure 4.17, the solutions to Eq. (4.15) provide a good qualitative description of this hysteretic behavior and the high-density steady states that are achieved. Similar hysteresis is also predicted and observed as a function of the RF drive voltage, V_{RW}.[5]

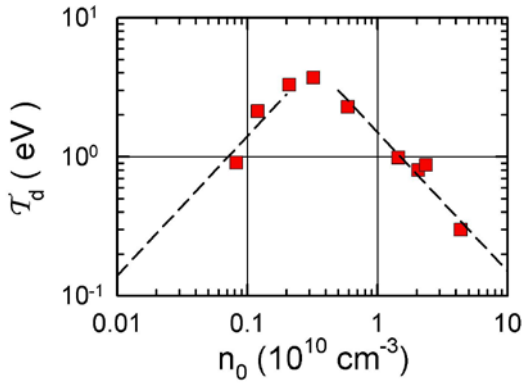

Fig. 4.18. Drag torque τ_d as a function of plasma density n_0 derived from the expansion data shown in Figure 4.11 for L_p = 24 cm. Dashed lines are guides to the eye. This dependence of τ_d on n_0 motivated the specific form of the second term in Eq. (4.15).

A key practical question is what limits the compression and the maximum achievable density. The UCSD experiments are routinely conducted with relative ease up to $f_{RW} \sim 8$ MHz and spottily up to ~ 18 MHz. This limit may be due to spurious resonances in the electronic circuitry or perhaps something more fundamental (e.g., the inability to couple effectively to the plasma at high frequencies); this will require further study to resolve.

RW compression in the single-particle regime. Low-density positron gases in Penning traps (i.e., collections of particles outside the plasma regime) have also been compressed using the RW technique with gas cooling.[100,102] For successful RW operation it was necessary that the particles be confined in a harmonic electrostatic potential well in the direction of the confining, uniform magnetic field. As shown in Figure 4.19, good compression was observed when $f_{RW} \leq \omega_z$, where ω_z is the axial bounce frequency in the harmonic well. In this case, it is believed that the particles couple to a rotating particle bounce resonance. As shown in Figure 4.19, at frequencies above ω_z, the particles are observed to heat rapidly and are de-confined.

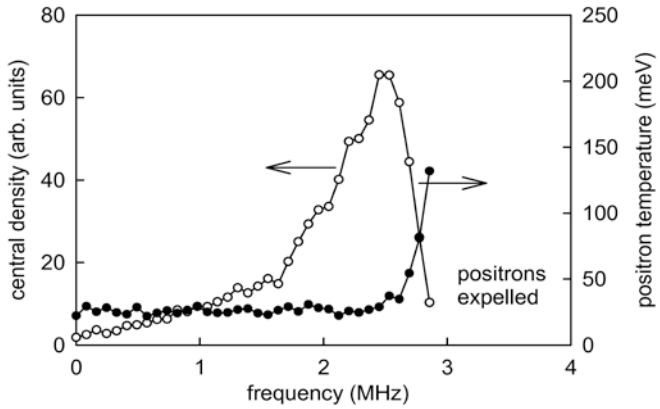

Fig. 4.19. Compression of a positron gas (i.e., in the single-particle regime) for an applied RW potential of 1.4 V. Good plasma compression is observed for f_{RW} at and below the axial bounce frequency of ω_z = 2.6 MHz. Above this frequency, plasma heating and particle expulsion are observed. The experiments use SF_6 for gas cooling. From reference[100]; see this reference for details.

The fact that the RW technique works in the single-particle regime is very useful in tailoring the charge clouds in buffer-gas traps, particularly ones that operate with fewer stages. In such traps, the cycle time must be kept short to avoid outward radial transport and annihilation, and hence the positron density is relatively low (i.e., the trapped positrons are in the single-particle, non-plasma regime).

Heating due to RW compression. Applying rotating electric fields to a plasma applies a torque τ_{RW} on it that heats the plasma by doing work on it. The heating rate can be written,[103]

$$P_H = \omega_{RW}\tau_{RW}, \tag{4.16}$$

where ω_{RW} is the angular frequency of the rotating electric field. In the strong-drive regime, the minimum power input to the plasma will be when the drive and drag torques are in balance, in which case $\omega_{RW} \approx \omega_E$ and $P_H = \omega_E \tau_{RW}$, where ω_E is the angular rotation frequency of the plasma.

The asymmetry-induced drag torque τ_a can be obtained by relating the time derivative of the plasma angular momentum (cf. Eq. (4.5)) to the outward expansion rate Γ_0.[81] Assuming a plasma of N particles with a flat-top density profile in surroundings at temperature T_W, the steady-state temperature T will be,[81]

$$T = T_W + \left(\frac{Ne^2}{3L_p}\right)\frac{\Gamma_0}{\Gamma_c}. \tag{4.17}$$

Illustrated in Figure 4.20 is the effect of plasma heating on RW compression. In this case the plasma is cooled by inelastic vibrational collisions with CF_4 molecules. Note that the temperature remains comparable to the ν_3 mode energy of 0.16 eV (i.e., the dominant positron-impact vibrational excitation) over an order of magnitude increase in the RW voltage. When it does break away from this value, as the RW voltage is increased further, the temperature rises rapidly and the maximum achievable compression decreases quickly.

Good compression is obtained as long as the collisional excitation of the ν_3 vibrational mode of CF_4 can control the plasma temperature. When

the temperature increases much above the energy of this excitation (ε_3 = 0.16 eV), then the temperature runs away and the compression is much less efficient.

Note that the plasma temperature, given by Eq. (4.17), is that expected for the minimum heating rate, which was obtained when the RW drive and asymmetry drag torque τ_a are balanced in the strong-drive regime. If there is "slip" (i.e., if $\omega_{RW} > \omega_E$), the heating rate will be larger. In this case, the excess heating rate due to the slip will be,

$$\delta P = \tau_{RW}\left(\omega_{RW} - 2\pi f_E\right) = 2\pi\tau_{RW}\Delta f \,, \tag{4.18}$$

where Δf is the so-called slip frequency.

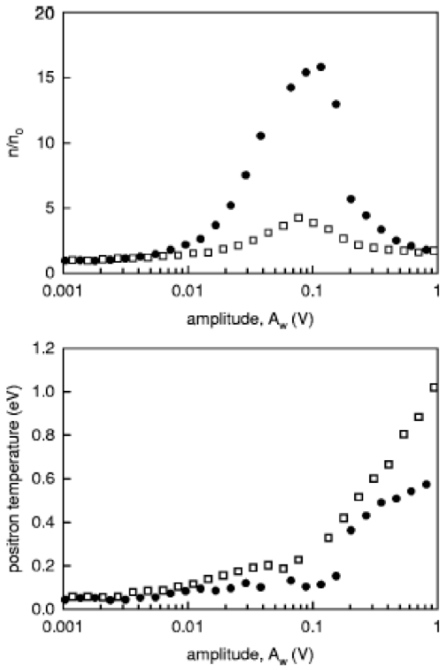

Fig. 4.20. Example of RW compression with gas cooling. Dependence of (above) the central density and (below) the positron temperature on RW drive amplitude, V_{RW} (labeled here as A_w), for cooling on CF_4 at pressures of (●) 3.5 x 10^{-8} mbar and (□) 8 x 10^{-9} mbar with f_{RW} = 2.5 MHz for 1 s. Reprinted from reference[7].

Maximum achievable density using RW compression. For many applications it is desirable to have as high a plasma density as possible. One constraint is the Brillouin limit. This limit arises from the fact that, for a particle in a PM trap rotating about the symmetry axis at frequency f_E, the v x B force acts both to provide the required inward centripetal force and to counteract the outward force due to the space-charge electric field. Due to the fact that the v x B force is proportional to the particle velocity v, and the centripetal force is proportional to v^2, this force balance is not possible above some maximum velocity v. And since the E x B rotation velocity, $v \propto n$, this imposes a maximum density limit, the so-called Brillouin limit.

The condition is[33]

$$\omega_p^2 = \omega_c^2/2, \tag{4.19}$$

where ω_p is the plasma frequency. The resulting Brillouin density limit is

$$n_B\left[m^3\right] = 4.8 \times 10^{18} B^2[T], \tag{4.20}$$

where n_B is in units of m^3 and B is in units of tesla. Above the Brillouin limit, particles at the plasma edge cannot be confined orbiting the axis of symmetry; they will move outward, unconfined.

However, if the plasma is in the presence of neutral gas molecules, even below this limit, any scattering will cause the particles to make relatively large cycloid-like orbits, moving outward on each collision an average distance, $E/\omega_c B$, where E is the space-charge electric field (cf. Figure 4.10). As the density increases, so will E, and hence the plasma will become more difficult to confine.

4.6. Concluding Remarks

The techniques described here have proven enormously useful in accumulating and manipulating positron, antimatter plasmas. They have played a central role in the quests to create low-energy antihydrogen and

the positronium molecule, Ps_2. They have also proven crucial in studies of atomic physics processes such as positron scattering and annihilation in interactions with atoms and molecules.

That said, there are likely many opportunities for further improvement. While there are a myriad of possibilities, here we mention just a few of the obvious ones. There are likely a number of ways to make buffer-gas positron traps simpler, more compact and, perhaps, more efficient. This might be done by clever design of the neutral gas profile and the differential pumping arrangement. There are also questions as to what limits the maximum trapping efficiency and how this can be improved. Finally, the range of atomic and molecular gases explored for trapping and cooling, while extensive, has not been exhaustive; there may well be room for further improvement here too.

Regarding the RW technique, it is presently uncertain what limits the maximum density that can be achieved, and this is a crucial issue for many applications. One question is: can one approach the Brillouin limit, and, if not, why not? There is also a question as to whether one might use a resonant structure to enhance greatly the cyclotron cooling.[73] If so, this will likely permit a broader range of operating parameters and the ability to operate at lower magnetic fields.

Acknowledgments

I would like to acknowledge the contributions of A. Passner, M. Leventhal, T. J. Murphy, M. Tinkle, R. G. Greaves, J. R. Danielson, E. A. Jerzewski and T. M. O'Neil to the work described here. I would also like to thank M. Charlton for his careful reading of the manuscript and helpful suggestions. This chapter relies heavily upon the data and descriptions in references[3–5,83,104]. This work is supported by the U.S. DOE/NSF Plasma Initiative.

References

1. C. M. Surko, J. R. Danielson, T. R. Weber, "Accumulation, Storage and Manipulation of Large Numbers of Positrons in Traps II - Selected Topics" in Knoop, M., Madsen, N. and Thompson, R. C. (eds), *Physics with Trapped Charged*

Particles (Imperial College Press, London, 2013), pp. XXX – YYY. (Reprinted with updates from reference[2].)

2. C. M. Surko, J. R. Danielson and T. R. Weber, "Accumulation, Storage and Manipulation of Large Numbers of Positrons in Traps II: selected topics" in Mills, A. P. and Dupasquier, A. (eds), *Physics with Many Positrons* (IOS press, Amsterdam, 2010), pp. 545–574.
3. C. M. Surko and R. G. Greaves, Emerging science and technology of antimatter plasmas and trap-based beams, *Phys. Plasmas* **11**, 2333–2348 (2004).
4. J. R. Danielson and C. M. Surko, "Plasma Compression using Rotating Electric Fields – the Strong Drive Regime", in Drewsen, M., Uggerhoj, U. and Knudsen, H. (eds), *Non-Neutral Plasma Physics* (American Institute of Physics Press, 2006), pp. 19–28.
5. J. R. Danielson, C. M. Surko and T. M. O'Neil, High-density Fixed Point for Radially Compressed Single-component Plasmas, *Phys. Rev. Lett.* **99**, 135005–135004 (2007).
6. J. H. Malmberg and C. F. Driscoll, Long-time containment of a pure electron plasma, *Phys. Rev. Lett.* **44**, 654–657 (1980).
7. R. G. Greaves and C. M. Surko, Radial compression and inward transport of positron plasmas using a rotating electric field, *Phys. Plasmas* **8**, 1879–1885 (2001).
8. J. Malmberg, T. M. O'Neil, A. W. Hyatt and C. F. Driscoll, presented at the Proceedings of the Sendai Symposium on Plasma Nonlinear Electron Phenomena, unpublished (1984) .
9. R. G. Greaves and C. M. Surko, Inward transport and compression of a positron plasma by a rotating electric field, *Phys. Rev. Lett.* **85**, 1883–1886 (2000).
10. J. R. Danielson and C. M. Surko, Torque-balanced high-density steady states of single component plasmas, *Phys. Rev. Lett.* **95**, 035001–035004 (2005).
11. R. Funakoshi, M. Amoretti, G. Bonomi, P. D. Bowe, C. Canali, C. Carraro, C. L. Cesar, M. Charlton, M. Doser, A. Fontana, M. C. Fujiwara, P. Genova, J. S. Hangst, R. S. Hayano, L. V. Jørgensen, A. Kellerbauer, V. Lagomarsino, R. Landua, E. L. Rizzini, M. Macrì, N. Madsen, G. Manuzio, D. Mitchard, P. Montagna, L. G. C. Posada, A. Rotondi, G. Testera, A. Variola, L. Venturelli, D. P. v. d. Werf, Y. Yamazaki and N. Zurlo, Positron plasma control techniques for the production of cold antihydrogen, *Phys. Rev. A* **76**, 012713–012718 (2007).
12. M. D. Tinkle, R. G. Greaves, C. M. Surko, R. L. Spencer and G. W. Mason, Low-order modes as diagnostics of spheroidal non-neutral plasmas, *Phys. Rev. Lett.* **72**, 352–355 (1994).
13. M. Amoretti, G. Bonomi, A. Bouchta, P. D. Bowe, C. Carraro and C. L. Cesar, Complete nondestructive diagnostic of nonneutral plasmas based on the detection of electrostatic modes, *Phys. Plasmas* **10**, 3056–3064 (2003).
14. J. R. Danielson, T. R. Weber and C. M. Surko, Extraction of Small-diameter Beams from Single-component Plasmas, *Appl. Phys. Lett.* **90**, 081503–081503 (2007).

15. T. R. Weber, J. R. Danielson and C. M. Surko, Creation of Finely Focused Particle Beams from Single–Component Plasmas, *Phys. Plasmas* **15**, 012106–012110 (2008).
16. T. R. Weber, J. R. Danielson and C. M. Surko, Energy Spectra of Tailored Particle Beams from Trapped Single–component Plasmas, *Phys. Plasmas* **16**, 057105–057108 (2009).
17. M. Amoretti, C. Amsler, G. Bonomi, A. Bouchta, P. Bowe, C. Carraro, C. L. Cesar, M. Charlton, M. Collier, M. Doser, V. Filippini, K. Fine, A. Fontana, M. Fujiwara, R. Funakoshi, P. Genova, J. Hangst, R. Hayano, M. Holzscheiter, L. Jorgensen, V. Lagomarsino, R. Landua, D. Lindelof, E. L. Rizzini, M. Macri, N. Madsen, G. Munuzio, M. Marchesotti, P. Montagna, H. Pruys, C. Regenfus, P. Riedler, J. Rochet, A. Rotondi, G. Rouleau, G. Testera, A. Variola, T. Watson and D. VanderWerf, Production and detection of cold antihydrogen atoms, *Nature* **419**, 456–459 (2002).
18. G. Gabrielse, N. Bowden, P. Oxley, A. Speck, C. Storry, J. Tan, M. Wessels, D. Grzonka, W. Oelert, G. Schepers, T. Sefzick, J. Walz, H. Pittner, T. Hansch and E. Hessels, Driven production of cold antihydrogen and the first measured distribution of antihydrogen states, *Phys. Rev. Lett.* **89**, 233401–233405 (2002).
19. G. Gabrielse, N. Bowden, P. Oxley, A. Speck, C. Storry, J. Tan, M. Wessels, D. Grzonka, W. Oelert, G. Schepers, T. Sefzick, J. Walz, H. Pittner, T. Hansch and E. Hessels, Background-free observation of cold antihydrogen with field-ionization analysis of its states, *Phys. Rev. Lett.* **89**, 213401–213404 (2002).
20. M. Amoretti, C. Amsler, G. Bonomi, A. Bouchta, P. D. Bowe, C. Carraro, M. Charlton, M. J. T. Collier, M. Doser, V. Filippini, K. S. Fine, A. Fontana, M. C. Fujiwara, R. Funakoshi, P. Genova, A. Glauser, D. Grögler, J. Hangst, R. S. Hayano, H. Higaki, M. H. Holzscheiter, W. Joffrain, L. V. Jørgensen, V. Lagomarsino, R. Landua, C. L. Cesar, D. Lindelöf, E. Lodi-Rizzini, M. Macri, N. Madsen, D. Manuzio, G. Manuzio, M. Marchesotti, P. Montagna, H. Pruys, C. Regenfus, P. Riedler, J. Rochet, A. Rotondi, G. Rouleau, G. Testera, D. P. v. d. Werf, A. Variola, T. L. Watson, T. Yamazaki and Y. Yamazaki, The ATHENA antihydrogen apparatus, *Nucl. Instrum. Methods A* **518**, 679–711 (2004).
21. V. Tsytovich and C. B. Wharton, Laboratory electron-positron plasma – a new research object, *Comments Plasma Phys. Controlled Fusion* **4**, 91–100 (1978).
22. R. G. Greaves and C. M. Surko, An electron-positron beam-plasma experiment, *Phys. Rev. Lett.* **75**, 3846–3849 (1995).
23. S. J. Gilbert, D. H. E. Dubin, R. G. Greaves and C. M. Surko, An electron-positron beam-plasma instability, *Phys. Plasmas* **8**, 4982–4994 (2001).
24. T. S. Pederson, A. H. Boozer, W. Dorland, J. P. Kremer and R. Schmitt, Prospects for the creation of positron-electron plasmas in a non-neutral stellarator, *J. Phys. B: At. Mol. Opt.* **36**, 1029–1039 (2003).
25. D. B. Cassidy, A. P. Mills, Jr., The Production of Molecular Positronium, *Nature* **449**, 195–197 (2007).
26. P. J. Schultz, K. G. Lynn, Interaction of positrons beams with surfaces, thin films, and interfaces, *Rev. Mod. Phys.* **60**, 701–779 (1988).

27. A. Dupasquier and A. P. Mills, *Positron Spectroscopy of Solids* (IOS Press, Amsterdam, 1995).
28. D. W. Gidley, D. Z. Chi, W. D. Wang and R. S. Vallery, Positron Annihilation as a Method to Characterize Porous Materials, *Ann. Rev. Mat. Sci.* **36**, 49–79 (2006).
29. R. G. Greaves and C. M. Surko, Positron trapping and the creation of high–quality trap–based positron beams, *Nucl. Instrum. Methods B* **192**, 90–96 (2002).
30. R. G. Greaves and J. M. Moxom, Recent results on trap-based positron beams, *Mat. Sci. Forum* **445–446**, 419–423 (2004).
31. R. L. Wahl, *Principles and Practice of Positron Emission Tomography* (Lippincott, Williams and Wilkins, Philadelphia, PA, 2002).
32. J. R. Danielson, T. R. Weber and C. M. Surko, Plasma Manipulation Techniques for Positron Storage, *Phys. Plasmas* **13**, 123502–123510 (2006).
33. R. C. Davidson, *Physics of Nonneutral Plasmas* (Addison-Wesley, Reading, MA, 1990).
34. D. H. E. Dubin and T. M. O'Neil, Trapped nonneutral plasmas, liquids, and crystals (the thermal equilibrium states), *Rev. of Mod. Phys.* **71**, 87–172 (1999).
35. A. P. Mills, Further improvements in the efficiency of low-energy positron moderators, *Appl. Phys. Lett.* **37**, 667–668 (1980).
36. A. P. Mills and E. M. Gullikson, Solid neon moderator for producing slow positrons, *Appl. Phys. Lett.* **49**, 1121–1123 (1986).
37. R. G. Greaves and C. M. Surko, Solid neon moderator for positron trapping experiments, *Can. J. Phys.* **51**, 445–448 (1996).
38. G. Gibson, W. C. Jordan and E. J. Lauer, Containment of positrons in a mirror machine, *Phys. Rev. Lett.* **5**, 141–144 (1960).
39. P. B. Schwinberg, J. R. S. Van Dyck and H. G. Dehmelt, Trapping and thermalization of positrons for geonium spectroscopy, *Phys. Lett.* **81A**, 119–120 (1981).
40. S. Chu and A. P. Mills, Excitation of the Positronium 1S –> 2S Two-Photon Transition, *Phys. Rev. Lett.* **48**, 1333–1336 (1982).
41. A. P. Mills, E. D. Shaw, R. J. Chichester and D. M. Zuckerman, Production of Slow Positron Bunches Using a Microtron Accellerator, *Rev. Sci. Instrum.* **60**, 825–830 (1989).
42. B. L. Brown, M. Leventhal, A. P. Mills and D. W. Gidley, Positron annihilation in a simulated low-density galactic environment, *Phys. Rev. Lett.* **53**, 2347–2350 (1984).
43. G. Gabrielse, L. Haarsma and S. L. Rolston, Open-endcap Penning traps for high precision experiments, *Int. J. Mass Spectrom.* **88**, 319–332 (1989).
44. H. Higaki and A. Mohri, Experiment on diocotron oscillations of spheroidal non–neutral electron plasmas in a multi-ring-electrode trap, *Phys. Lett. A* **235**, 504–507 (1997).
45. T. O'Neil, Plasmas with a single sign of charge (an overview), *Physica Scripta* **T59**, 341–351 (1995).
46. J. J. Bollinger, D. J. Wineland and D. H. E. Dubin, Non-neutral ion plasmas and crystals, laser cooling, and atomic, *Phys. Plasmas* **1**, 1403–1414 (1994).

47. T. M. O'Neil, A confinement theorem for nonneutral plasmas, *Phys. Fluids* **23**, 2216–2218 (1980).
48. D. Segers, J. Paridaens, M. Dorikens and L. Dorikens–Vanpraet, Beam handling with a Penning trap of a LINAC-based slow positron beam, *Nucl. Instrum. Methods* **A337**, 246–252 (1994).
49. R. G. Greaves, M. D. Tinkle and C. M. Surko, Creation and uses of positron plasmas, *Phys. Plasmas* **1**, 1439–1446 (1994).
50. L. V. Jørgensen, M. Amoretti, G. Bonomi, P. D. Bowe, C. Canali, C. Carraro, C. L. Cesar, M. Charlton, M. Doser, A. Fontana, M. C. Fujiwara, R. Funakoshi, P. Genova, J. S. Hangst, R. S. Hayano, A. Kellerbauer, V. Lagomarsino, R. Landua, E. L. Rizzini, M. Macrì, N. Madsen, D. Mitchard, P. Montagna, A. Rotondi, G. Testera, A. Variola, L. Venturelli, D. P. v. d. Werf and Y. Yamazaki, New Source of Dense, Cryogenic Positron Plasmas, *Phys. Rev. Lett.* **95**, 025002–025005 (2005).
51. C. M. Surko, M. Leventhal and A. Passner, Positron plasma in the laboratory, *Phys. Rev. Lett.* **62**, 901–904 (1989).
52. T. J. Murphy and C. M. Surko, Positron trapping in an electrostatic well by inelastic collisions with nitrogen molecules, *Phys. Rev. A* **46**, 5696–5705 (1992).
53. B. M. Jelenkovic, A. S. Newbury, J. Bollinger, W. M. Itano and T. B. Mitchell, Sympathetically cooled and compressed positron plasma, *Phys. Rev. A* **67**, 063406–063409 (2003).
54. N. Oshima, T. M. Kojima, M. Niigati, A. Mohri, K. Komaki and Y. Yamazaki, New scheme for positron accumulation in ultrahigh vacuum, *Phys. Rev. Lett.* **93**, 195001–195004 (2004).
55. H. Boehmer, M. Adams and N. Rynn, Positron trapping in a magnetic mirror configuration, *Phys. Plasmas* **2**, 4369–4371 (1995).
56. L. Haarsma, K. Abdullah and G. Gabrielse, Extremely cold positrons accumulated, *Phys. Rev. Lett.* **75**, 806–809 (1995).
57. J. Estrada, T. Roach, J. N. Tan, P. Yesley and G. Gabrielse, Field ionization of strongly magnetized Rydberg positronium: A new physical mechanism for positron accumulation, *Phys. Rev. Lett.* **84**, 859–862 (2000).
58. B. Ghaffari and R. S. Conti, Experimental evidence for chaotic transport in a positron trap, *Phys. Rev. Lett.* **75**, 3118–3121 (1995).
59. R. G. Greaves and J. Moxom, "Design and Performance of a Trap-Based Beam Source" in Schauer, M., Mitchell, T. and Nebel, R. (eds), *Non-Neutral Plasma Physics V* (American Institute of Physics, New York, 2003), pp. 140–148.
60. C. M. Surko, A. Passner, M. Leventhal and F. J. Wysocki, Bound states of positrons and large molecules, *Phys. Rev. Lett.* **61**, 1831–1834 (1988).
61. J. P. Marler and C. M. Surko, Positron-impact ionization, positronium formation and electronic excitation cross sections for diatomic molecules, *Phys. Rev. A* **72**, 062713–062710 (2005).
62. J. P. Marler and C. M. Surko, Systematic comparison of positron and electron impact excitation of the ν_3 vibrational mode of CF_4, *Phys. Rev. A* **72**, 062702–062706 (2005).

63. C. M. Surko, S. J. Gilbert, and R. G. Greaves, "Progress in Creating Low-Energy Positron Plasmas and Beams" in Bollinger, J. J., Spencer, R. L., and Davidson, R. C. (eds), *Non-Neutral Plasma Physics* (American Institute of Physics, New York, 1999), pp. 3–12.
64. J. Clarke, D. P. v. d. Werf, B. Griffiths, D. C. S. Beddows, M. Charlton, H. H. Telle and P. R. Watkeys, Design and operation of a two-stage positron accumulator, *Rev. Sci. Instrum.* **77**, 063302–063305 (2006).
65. C. M. Surko, G. F. Gribakin and S. J. Buckman, Low-energy positron interactions with atoms and molecules, *J. Phys. B: At. Mol. Opt. Phys.* **38**, R57–R126 (2005).
66. A. Bankovic, J. P. Marler, M. Suvakov, G. Malovic and Z. L. Petrovic, Transport Coefficients for Positron Swarms in Nitrogen, *Nuc. Instrum. Methods B* **266**, 462–465 (2008).
67. S. J. Gilbert, R. G. Greaves and C. M. Surko, Positron scattering from atoms and molecules at low energies, *Phys. Rev. Lett.* **82**, 5032–5035 (1999).
68. J. Sullivan, S. J. Gilbert and C. M. Surko, Excitation of Molecular Vibrations by Positron Impact, *Phys. Rev. Lett.* **86**, 1494–1497 (2001).
69. J. P. Marler, G. Gribakin and C. M. Surko, Comparison of positron-impact vibrational excitation cross sections with the Born-dipole model, *Nucl. Instrum. Methods B* **247**, 87–91 (2006).
70. I. Al-Qaradawi, M. Charlton and I. Borozan, Thermalization times of positrons in molecular gases, *J. Phys. B* **33**, 2725–2732 (2000).
71. P. G. Coleman, T. C. Griffith and G. R. Heyland, Rotational-excitation and momentum-transfer in slow positron-molecule collisions, *J. Phys. B* **14**, 2509–2517 (1981).
72. B. R. Beck, J. Fajans and J. H. Malmberg, Measurement of collisional anisotropic temperature relaxation in a strongly magnetized pure electron plasma, *Phys. Rev. Lett.* **68**, 317–320 (1992).
73. T. M. O'Neil, Cooling of a pure electron plasma by cyclotron radiation, *Phys. Fluids* **23**, 725–731 (1980).
74. M. D. Tinkle, R. G. Greaves and C. M. Surko, Low-order longitudinal modes of single-component plasmas, *Phys. Plasmas* **2**, 2880–2894 (1995).
75. M. Amoretti, C. Amsler, G. Bonomi, A. Bouchta, P. D. Bowe, C. Carraro, C. L. Cesar, M. Charlton, M. Doser, V. Filippini, A. Fontana, M. C. Fujiwara, R. Funakoshi, P. Genova, J. S. Hangst, R. S. Hayano, L. V. Jørgensen, V. Lagomarsino, R. Landua, D. Lindelöf, E. L. Rizzin, M. Macrí, N. Madsen, G. Manuzio, P. Montagna, H. Pruys, C. Regenfus, A. Rotondi, G. Testera, A. Variola and D. P. v. d. Werf, Positron Plasma Diagnostics and Temperature Control for Antihydrogen Production, *Phys. Rev. Lett.* **91**, 05501–05505 (2003).
76. D. J. Griffiths, *Introduction to Electrodynamics* (Prentice Hall, Saddle River, NJ, 1981).
77. F. F. Chen, *Introduction to Plasma Physics and Controlled Fusion, Volume I: Plasma Physics*, Second edition (Springer, New York, 1984).
78. T. M. O'Neil and D. H. E. Dubin, Thermal Equilibria and Thermodynamics of Trapped Plasmas with a Single Sign of Charge, *Phys. Plasmas* **5**, 2163–2193 (1998).

79. C. F. Driscoll and J. H. Malmberg, Length-dependent containment of a pure electron-plasma column, *Phys. Rev. Lett.* **50**, 167–170 (1983).
80. A. A. Kabantsev and C. F. Driscoll, Trapped-particle Mediated Collisional Damping of Nonaxisymmetric Plasma Waves, *Phys. Rev. Lett.* **97**, 095001–095004 (2006).
81. J. R. Danielson and C.M. Surko, Radial Compression and Torque-balanced Steady States of Single-Component Plasmas in Penning-Malmberg traps, *Phys. Plasmas* **13**, 055706–055710 (2006).
82. E. M. Hollmann, F. Anderegg and C. F. Driscoll, Confinement and Manipulation of Non-neutral Plasmas Using Rotating Wall Electric Fields, *Phys. Plasmas* **7**, 2776–2789 (2000).
83. C. M. Surko and R. G. Greaves, A multi-cell trap to confine large numbers of positrons, *Rad. Chem. and Phys.* **68**, 419–425 (2003).
84. O. Sueoka, H. Takak, A. Hamada, H. Sato and M. Kimura, Total cross sections of electron and positron collisions with CHF_3 molecules: a comparative study with CH4 and CF4, *Chem. Phys. Lett.* **288**, 124–130 (1998).
85. X. P. Huang and C. F. Driscoll, Relaxation of 2D Turbulence to a Metaequilibrium Near the Minimum Enstrophy State, *Phys. Rev. Lett.* **72**, 2187–2190 (1994).
86. R. Spencer, G. W. Mason, and S. N. Rasband, "Numerical Non-Neutral Plasmas" in Schauer, M., Mitchell, T. and Nebel, R. (eds), *Non-Neutral Plasma Physics V* (American Institute of Physics Press, Melville, New York, 2003).
87. D. L. Eggleston, C. F. Driscoll, B. R. Beck, A. W. Hyatt and J. H. Malmberg, Parallel energy analyzer for pure electron plasma devices, *Phys. Fluids B* **4**, 3432–3439 (1992).
88. J. S. Degrassie and J. H. Malmberg, Wave-induced transport in pure electron-plasma, *Phys. Rev. Lett.* **39**, 1077–1080 (1977).
89. K. S. Fine and C. F. Driscoll, The finite length diocotron mode, *Phys. Plasmas* **5**, 601–607 (1998).
90. D. H. E. Dubin, Theory of electrostatic fluid modes in a cold spheroidal non-neutral plasma, *Phys. Rev. Lett.* **66**, 2076–2079 (1991).
91. C. S. Weimer, J. J. Bollinger, F. L. Moore and D. J. Wineland, Electrostatic modes as a diagnostic in Penning trap experiments, *Phys. Rev. A* **49**, 3842–3853 (1994).
92. F. Anderegg, N. Shiga, J. R. Danielson, D. H. E. Dubin, C. F. Driscoll and R. W. Gould, Thermally excited modes in a pure electron plasma, *Phys. Rev. Lett.* **90**, 115001–115001 (2003).
93. N. Oshima, T. M. Kojima, M. Niigaki, A. Mohri, K. Komaki, Y. Iwai and Y. Yamazaki, Development of a cold HCI source for ultra-slow collisions, *Nucl. Instr. Methods B* **205**, 178–182 (2003).
94. X. P. Huang, F. Anderegg, E. M. Hollmann, C. F. Driscoll and T. M. O'Neil, Steady state confinement of nonneutral plasma by rotating electric fields, *Phys. Rev. Lett.* **78**, 875–878 (1997).
95. X. P. Huang, J. J. Bollinger, T. B. Mitchell and W. M. Itano, Phase-locked rotation of crystallized non-neutral plasmas by rotating electric fields, *Phys. Rev. Lett.* **80**, 73–76 (1998).

96. T. B. Mitchell, J. J. Bollinger, W. M. Itano and D. H. E. Dubin, Stick-slip dynamics of a stressed ion crystal, *Phys. Rev. Lett.* **87**, 183001–183001 (2001).
97. J. J. Bollinger, T. B. Mitchell, X.-P. Huang, W. M. Itano, J. N. Tan, B. M. Jelenkovic and D. J. Wineland, Crystalline order in laser–cooled, non-neutral ion plasmas, *Phys. Plasmas* **7**, 7 (2000).
98. F. Anderegg, E. M. Hollmann and C. F. Driscoll, Rotating field confinement of pure electron plasmas using Trivelpiece-Gould modes, *Phys. Rev. Lett.* **81**, 4875–4878 (1998).
99. D. P. Vanderwerf, M. Amoretti, G. Bonomi, A. Bouchta, P. D. Bowe, C. Carraro, C. L. Cesar, "Transfer, Stacking, and Compression of Positronn Plasmas under UHV conditions" in Schauer, M., Mitchell, T. and Nebel, R. (eds), *Non-Neutral Plasma Physics V* (American Institute of Physics Press, Melville, New York, 2003), pp. 172–177.
100. R. G. Greaves and J. M. Moxom, Compression of Trapped Positrons in a Single Particle Regime by a Rotating Electric Field, *Phys. Plasmas* **15**, 072304–072306 (2008).
101. J. R. Danielson, P. Schmidt, J. P. Sullivan, C. M. Surko, "A Cryogenic, High-Field Trap for Large Positron Plasamas and Cold Beams" in Schauer, M., Mitchell, T. and Nebel, R. (eds), *Non-Neutral Plasma Physics V* (American Institute of Physics Press, Melville, New York, 2003) pp. 149–161.
102. C. A. Isaac, C. J. Baker, T. Mortensen, D. P. v. d. Werf and M. Charlton, Compression of Positron Clouds in the Independent Particle Regime, *Phys. Rev. Lett.* **107**, 033201–033204 (2011).
103. R. W. Gould, "Wave Angular Momentum in Nonneutral Plasmas" in Bollinger, J. J., Spencer, R. L. and Davidson, R. C. (eds), *Conference Proceedings No. 498, Non-Neutral Plasma Physics III* (American Institute of Physics, Melville, New York, 1999), pp. 170–175.
104. R. G. Greaves and C. M. Surko, Antimatter plasmas and antihydrogen, *Phys. Plasmas* **4**, 1528–1543 (1997).